Journal of Biomolecular NMR, 8 (1996) 369–378
ESCOM



J-Bio NMR 396

# Dynamic studies of a fibronectin type I module pair at three frequencies: Anisotropic modelling and direct determination of conformational exchange

Isabelle Q.H. Phan*, Jonathan Boyd and Iain D. Campbell

*Oxford Centre for Molecular Sciences and Department of Biochemistry, University of Oxford, South Parks Road, Oxford OX1 3QU, U.K.*

Received 11 June 1996
Accepted 20 September 1996

*Keywords:* Dynamics; Multiple fields; Anisotropy; Conformational exchange

**Summary**

A detailed analysis of the $^{15}N$ relaxation of a pair of modules from fibronectin is presented. The overall dimensions of the protein structure can be approximated by a cylinder with an axial ratio $D_{\parallel}/D_{\perp}$ of 1.9. $T_1$, $T_2$ and NOE data, collected at three $^{15}N$ frequencies (50.6, 60.8 and 76 MHz), can be fitted satisfactorily to a Lipari–Szabo model, taking anisotropy into account. A method for analysing the exchange contribution to relaxation is presented. This contribution depends upon the predicted $B_0^2$ frequency dependence in the fast exchange limit of these exchange terms. Using this analysis, relatively slow conformational exchange contributions are detected around one of the disulphide bonds in the first module of the pair.

## Introduction

Recent reviews have illustrated the current interest in the biological and structural aspects of modular proteins (Campbell and Downing, 1994; Bork and Bairoch, 1995; Pawson, 1995; Bork et al., 1996). Fibronectin, an archetypal mosaic protein that is almost entirely constituted of three types of modules, is an extracellular matrix protein involved in many important biological processes (for a review see Potts and Campbell, 1994). The main fibrin binding site has been located to the fourth and fifth fibronectin type I modules ($^4$F1$^5$F1) of the N-terminal region of fibronectin (Matsuka et al., 1994; Rostagno et al., 1994). The structure of this module pair (93 residues) has been determined by high-resolution NMR spectroscopy (Williams et al., 1994). Each of the two modules composing the pair was shown to retain the characteristic fold of single fibronectin type I modules. Subsequent fluorescent studies have supported the evidence from NMR that the two modules are linked by a tight hydrophobic interface and that the $^4$F1$^5$F1 pair, joined together by a five-residue linker, forms an overall rigid structure (Matsuka et al., 1994). To elucidate further the dynamic behaviour of this module pair in solution, relaxation studies on a $^{15}N$-labelled sample were undertaken and the results are presented here. We show that, from the analysis of $^{15}N$ relaxation rates, the $^4$F1$^5$F1 molecule can be satisfactorily modelled as a rigid cylinder with an axial ratio significantly larger than those reported for proteins previously analysed by anisotropic rotational diffusion models. The analysis has been facilitated by collecting experimental data at three frequencies. A model-free approach has been used to determine experimentally those sites whose relaxation is affected by rapid conformational exchange. This approach also provides a method to calculate the exchange contribution to the transverse relaxation directly from the experimental data.

## Collection of $^{15}N$ NMR relaxation data

Relaxation experiments were performed at $^{15}N$ frequencies of 50.6, 60.8 and 76.0 MHz on a uniformly $^{15}N$-labelled sample of a recombinant fibronectin type I fourth and fifth module pair ($^4$F1$^5$F1). The sample conditions were approximately 500 μM in 5% $D_2O$/95% $H_2O$, pH 4.6, 37 °C. The sample was degassed with $N_2$ by concen-

*To whom correspondence should be addressed.
*Supplementary Material:* $^{15}N$ assignments of residues in $^4$F1$^5$F1 and experimental $T_1$ and $T_2$ data are available upon request from the authors.

trating it with an Amicon Ultrafiltration cell, and it was kept in a sealed Taperlok™ Wilmad NMR tube. Measurements of relaxation data were carried out using previously described methods, modified where possible to include pulsed field gradients (Kay et al., 1989; Boyd et al., 1990; Farrow et al., 1994). Spectral widths at all frequencies were 12 500.00 Hz in F2 and 24.9 ppm for $^{15}N$. The $^{1}H$ and $^{15}N$ carriers were positioned on the $H_2O$ resonance and at 117.6 ppm, respectively. Resonance assignments for backbone amide $^{15}N$ are provided in the Supplementary Material.

For $T_1$ and $T_2$ experiments, 2K complex data points were collected in F2 and 44, 52 and 64 complex $t_1$ increments of 96 scans with a recycle delay of 2 s were acquired at 50.6, 60.8 and 76.0 MHz, respectively. Relaxation delays used for the collection of $T_1$ and $T_2$ relaxation rates are presented in Table 1. For the measurement of $T_2$, the delay between 180° pulses in the CPMG sequence ($2\tau$) was set to 650 μs. $^{15}N$ rf field strengths were 5.2, 5.5 and 5.2 kHz at 750, 600 and 500 MHz, respectively. The widths of the 180° CPMG pulses were 96, 90 and 96 μs at 50.6, 60.8 and 76.0 MHz $^{15}N$ frequency, respectively. The relaxation times $T_1$ and $T_2$ were obtained from two-parameter exponential fits of resonance intensities. The heteronuclear Overhauser experiment ($^{15}N$-{$^{1}H$} NOE) was recorded at 50.6 and 76.0 MHz $^{15}N$ frequency. A total of 1024 complex data points were collected in F2; 44 complex $t_1$ increments of 384 scans were recorded at 50.6 MHz, and 54 complex $t_1$ increments of 256 scans at 76.0 MHz. In all cases the relaxation delays were chosen to be four to five times the $^{15}N$ $T_1$, ensuring solvent recovery and complete NOE (e.g. at 750 MHz this was 4.5 s). In each case, one spectrum with the NOE and one without were collected. The NOE effect was calculated as the ratio of resonance intensities in spectra collected with and without NOE.

All data sets were deconvoluted in F2 with a Lorentzian to Gaussian lineshape window function. In F1, a 90°-shifted sine-bell apodisation was applied after linear prediction to twice the number of recorded complex $t_1$ points. The data were processed using the FELIX program (Biosym Technologies, San Diego, CA, U.S.A.) and analysed with the Modelfree program developed by A. Palmer. Errors in $T_1$ and $T_2$ values were approximated by two standard deviations of the baseline noise level. Errors on $^{15}N$-{$^{1}H$} NOE values were estimated from a Monte Carlo simulation, which used two standard deviations of baseline noise.

## Analysis of $^{15}N$ relaxation data

To decide on a suitable rotational diffusion model to fit the experimental data, it was first assumed that the molecule tumbled isotropically. The results obtained were then compared with those from data fitting using an individual overall correlation time for each residue, which is equivalent to fitting the data to an anisotropic diffusor.

The data were first analysed using the simple model-free formalism developed by Lipari and Szabo assuming an isotropically tumbling molecule (Abragam, 1961; Lipari and Szabo, 1982). In this approach, four parameters describing dynamic motions, $S^2$, $\tau_m$, $\tau_e$ and $R_{ex}$, are extracted from the equations relating the $T_1$, $T_2$ and $^{15}N$-{$^{1}H$} NOE to the spectral density function (Kay et al., 1989); $\tau_m$ is the overall rotational correlation time for a spherical molecule, $S^2$ is a generalised order parameter measuring the degree of spatial restriction of rapid internal motions of the N-H bond vector, $\tau_e$ is the rate of these rapid internal motions and $R_{ex}$ is the term accounting for chemical exchange. The extended model-free formula (Clore et al., 1990) was not used, as it has recently been shown on simulated data to introduce fictitious slow internal motion to compensate for motional anisotropy (Schurr et al., 1994). Each residue was assigned to one of four dynamic models, which used the following combinations of parameters: (1) $S^2$; (2) $S^2$, $R_{ex}$; (3) $S^2$, $\tau_e$; (4) $S^2$, $R_{ex}$, $\tau_e$. The assignment of the individual $^{15}N$ data to either of these four classes was based on statistical considerations. The data were first fitted using each of the models with a $\tau_m$ restricted to the range $4.6 \pm 0.5$ ns, estimated from the average $T_1/T_2$ ratio of those residues that had neither significant shortening of $T_2$ nor a $^{15}N$-{$^{1}H$} NOE value less than 0.6 at 76.0 MHz $^{15}N$ frequency. The statistically best fitting model for individual residues was then used to optimise $\tau_m$. This analysis fitted the relaxation data for only 32 (39%) residues, giving an overall

TABLE 1
RELAXATION DELAYS FOR THE EXPERIMENTAL DETERMINATION OF $T_1$ AND $T_2$ FOR $^{4}F1^{5}F1$

| $^{15}N$ frequency (MHz) | Relaxation delays (ms) | |
|---|---|---|
| | $T_1$ | $T_2$ |
| 50.7 | 20.04, 80.15, 140.25, 200.36, 300.55, 400.73, 500.91, 601.09 | 5.97, 17.90, 29.84, 41.78, 59.68, 77.58, 89.52, 119.36, 149.20, 173.07, 179.04 |
| 60.8 | 20.03, 100.17, 200.35, 300.52, 500.87, 601.04, 801.39, 901.57 | 5.92, 17.76, 41.44, 59.20, 118.40, 148.00, 236.80 |
| 76.0 | 20.04, 100.20, 200.40, 300.60, 400.80, 501.00, 601.20, 801.60, 1002.00, 1202.40 | 5.97, 23.87, 41.78, 59.68, 89.52, 119.36, 149.20, 179.04 |

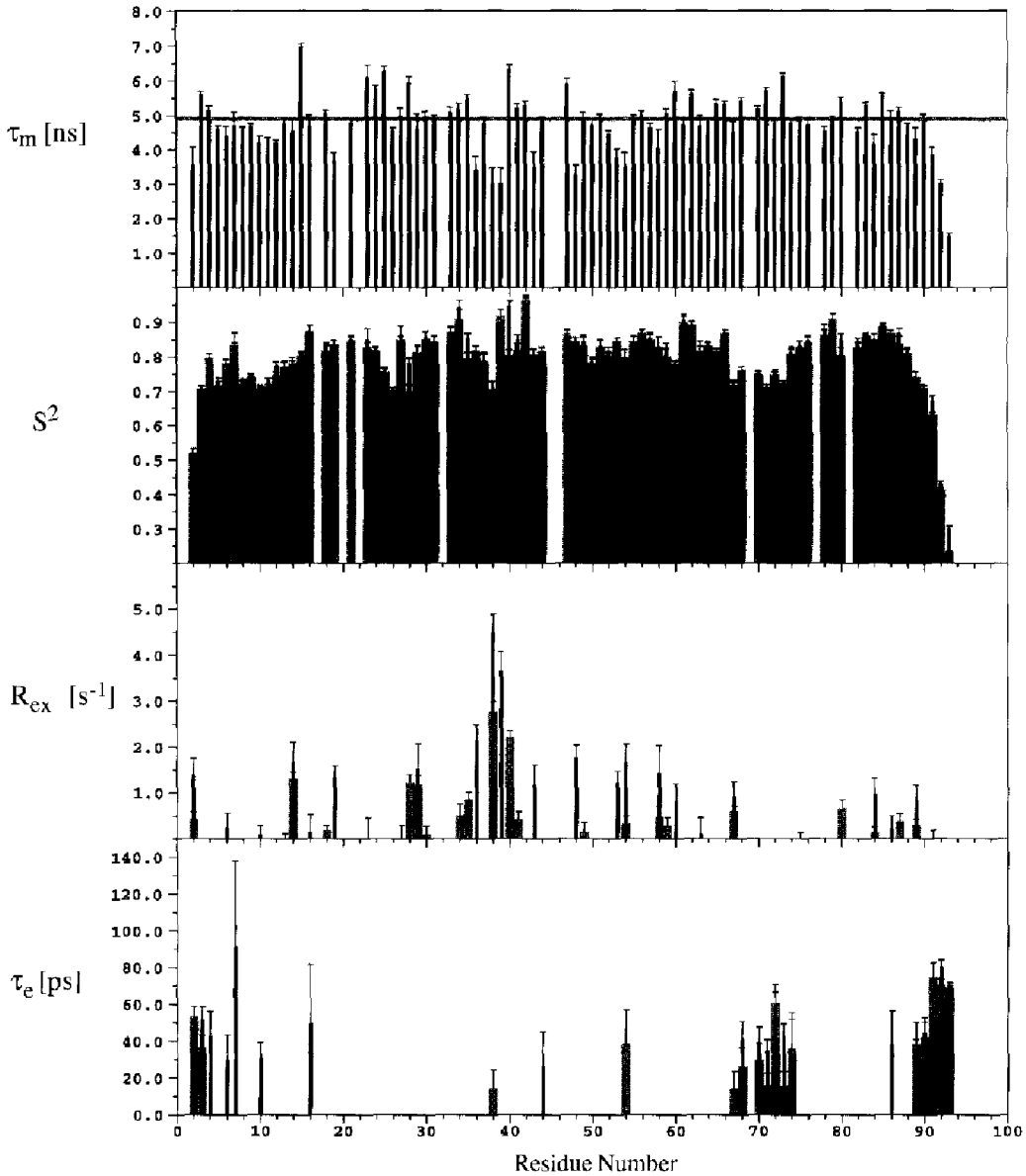


Fig. 1. Summary of relaxation parameter fitting for $^4$F1$^5$F1 using the simple isotropic Lipari–Szabo model (black bars) and the Lipari–Szabo model with variable $\tau_m$ (grey bars), as a function of the residue number. From top to bottom: overall correlation time (the grey horizontal bar at 4.9 ns represents the fixed optimised correlation time used in the isotropic fitting); order parameter $S^2$; chemical exchange term $R_{ex}$; fast-motion correlation time $\tau_e$.

rotational correlation time $\tau_m$ of $4.90 \pm 0.01$ ns. However, when the fitting procedure was repeated using a variable $\tau_m$, which is equivalent to introducing rotational anisotropy, an additional 16 (52%) residues were fitted and the resulting $\tau_m$ values ranged from 3.02 to 7.00 ns. Results for both isotropic and modified Lipari–Szabo models are presented in Fig. 1 and the corresponding residual errors on the $T_1/T_2$ data are shown in Figs. 2A and B, respectively. In accordance with recent theoretical models (Schurr et al., 1994), introducing a variable $\tau_m$ did not significantly alter the $S^2$ data obtained from isotropic fitting, despite large variations in $\tau_m$ values. The same applies to the parameter for fast internal motions, $\tau_e$; both models locate rapid motion to the N- and C-terminal ends, and to the second to last loop of the double module (residues 68–74). Note that no fast motion was detected in the linker region (residues 44–48) between the two modules of the $^4$F1$^5$F1 module pair, as no decrease in the $^{15}$N-{$^1$H} NOE was observed for the three linker residues for which NOE data was available (see Fig. 3). This is in marked contrast to the sharp 'dip' in the NOE values observed for the flexible hinge of calmodulin (Barbato et al., 1992) and indicates that $^4$F1$^5$F1 behaves as a rigid body on the (sub)nanosecond time scale. Unlike the $\tau_e$ data, large discrepancies were found for exchange contributions, $R_{ex}$, with no consistent pattern emerging from either fitting method. In fact, the attribution of an exchange term seemed to be almost random, illustrating the

need to assess exchange rates independently. It seems clear, however, from both statistical considerations and the large spread in $\tau_m$ values obtained in the variable $\tau_m$ analysis, that the interpretation of the experimental data requires the inclusion of anisotropic rotational diffusion.

The modified Lipari–Szabo model with variable $\tau_m$ provides a simple method for detecting anisotropic rotational diffusion. In this case, the parameter $\tau_m$ is a fairly sensitive function of the direction of the NH internuclear vector with respect to the rotational diffusion tensor (Barbato et al., 1992; Brüschweiler et al., 1995). Therefore, we applied a more elaborate treatment of anisotropy

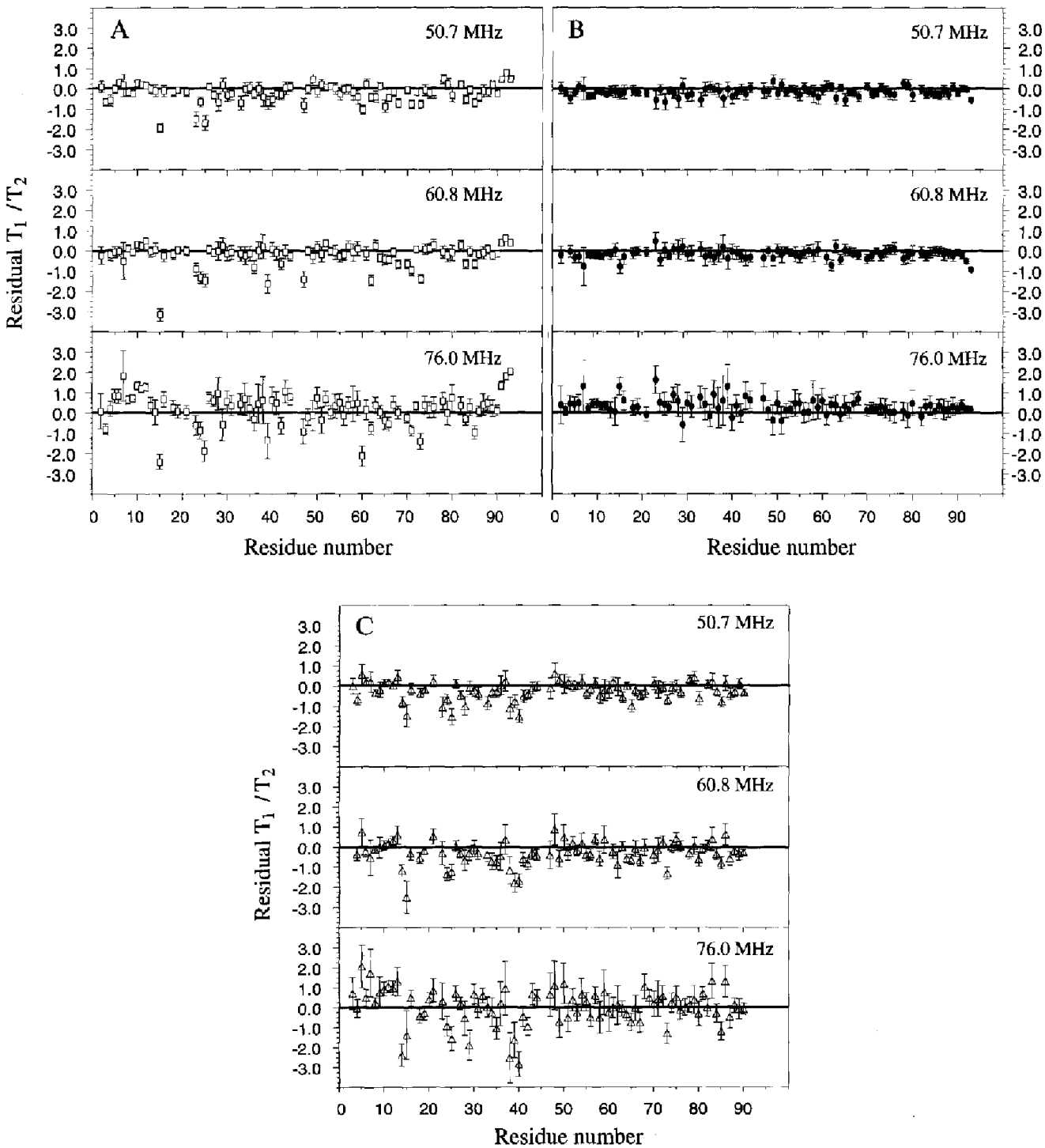


Fig. 2. Residual errors of relaxation parameter fitting for $^4$F1$^5$F1, plotted as the difference between the calculated and experimental $T_1/T_2$ data, for (A) the simple isotropic Lipari–Szabo model; and (B) the Lipari–Szabo model with variable $\tau_m$. (C) Residual errors on $T_1/T_2$ data from anisotropy fitting with the beads model. Note that, unlike in the Lipari–Szabo model, no $R_{ex}$ or $\tau_e$ term was included in the fitting procedures in this case, and therefore these data cannot be readily compared with data presented in (A) and (B).

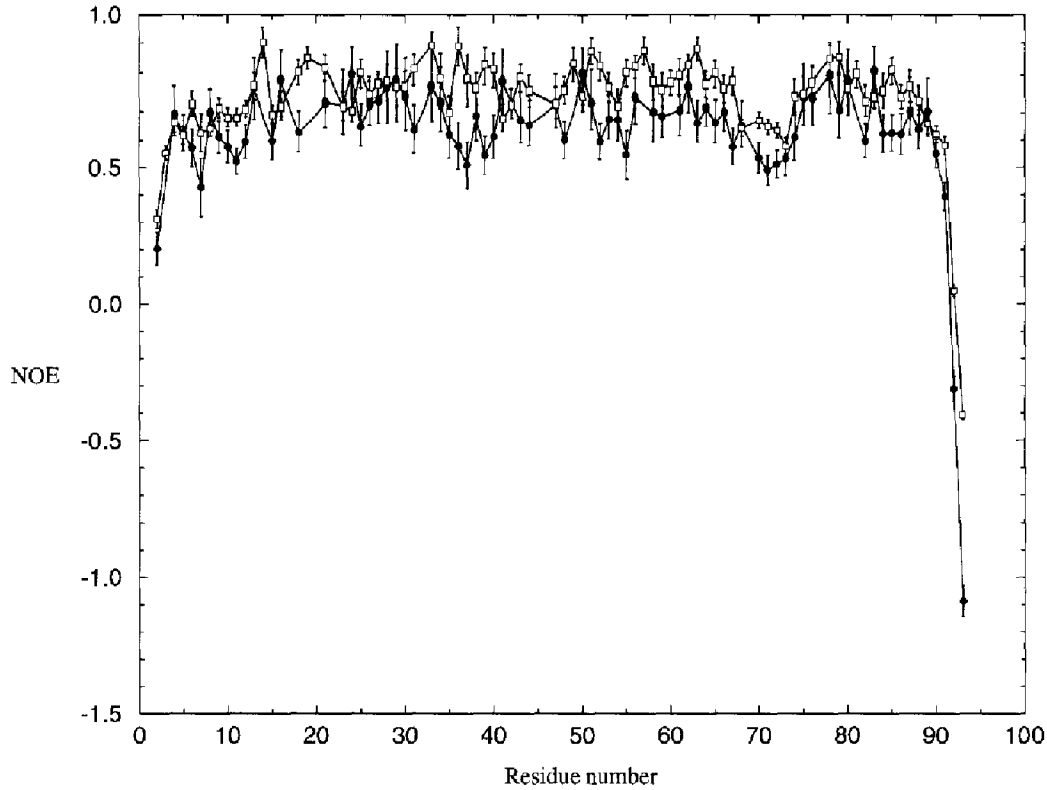


Fig. 3. Heteronuclear Overhauser experiment ($^{15}$N-{$^{1}$H} NOE). Experimental data at $^{15}$N frequencies of 50.6 and 76.0 MHz are shown as filled circles and open squares, respectively. Error values estimated from a Monte Carlo simulation are shown as bars and whiskers.

in relaxation measurements, which has been described previously (Woessner, 1962a). Briefly, it requires the use of a modified spectral density function with five correlation times; these depend on the three distinct eigenvalues of the rotational diffusion tensor which describes the rotational motion of the molecule in solution. In the case of cylindrical symmetry, the number of correlation times reduces to three; the rotational diffusion of the cylindrical molecule is then described by the two distinct eigenvalues of the rotational diffusion tensor, $D_{\parallel}$ and $D_{\perp}$, which correspond to the rotational diffusion parallel and perpendicular to the main axis of cylindrical symmetry, respectively. The degree of anisotropy of $^{4}$F1$^{5}$F1 was first estimated by calculating the ratio of the three components of the inertia tensor from the average solution structure: the result, 4.60:4.29:1.00, clearly indicates that the molecule can be modelled as a cylinder. In this case, the spectral density function is affected by the orientation of the amide N-H bond vector relative to the main axis of rotational diffusion and is therefore expressed as a function of the angle between the N-H vector and $D_{\parallel}$ (Woessner, 1962b). It was assumed that this expression for the spectral density function could be used for both dipolar and chemical shift anisotropy, since the chemical shift tensor lies in the peptide plane and forms an angle of 20° or less with the backbone amide bond (Oas et al., 1987). Practically, anisotropy can then be measured as a fluctuation in the $T_1/T_2$ ratios: lower $T_1/T_2$ ratios are found for residues where the backbone amide bond is perpendicular to $D_{\parallel}$, the main component of the cylindrical rotational diffusion tensor, and higher $T_1/T_2$ values when the amide bond is parallel to $D_{\parallel}$. Anisotropic rotational diffusion for $^{4}$F1$^{5}$F1 was therefore modelled by back-calculating the $T_1/T_2$ ratio from the rotational diffusion tensor for a cylindrical molecule, and the angle $\alpha$ between each backbone amide bond and $D_{\perp}$ (Barbato et al., 1992; Zheng et al., 1995). The average $T_1/T_2$ ratios and standard deviations were calculated over an ensemble of 32 $^{4}$F1$^{5}$F1 structures obtained by simulated annealing (Williams et al., 1994).

The rotational diffusion constants for all 32 structures were calculated using the bead model of García de la Torre and Bloomfield (García de la Torre and Bloomfield, 1981; García de la Torre et al., 1994). Each of the residues 3–90, corresponding to the rigid cylindrical core of the protein, was modelled by a single bead centred on the $C^{\alpha}$ atom. The viscosity was set to 0.0006947 kg m$^{-1}$ s$^{-1}$, which corresponds to the viscosity of water at 37 °C. A grid search was performed to optimise the bead radius, so that the back-calculated $T_1/T_2$ values best fitted the experimental $T_1/T_2$ data. The optimised bead radius was 3.0 Å. No water shell was needed to fit the data, in apparent contradiction to earlier models for determining rotational diffusion constants of proteins (Venable and Pastor, 1988). However, modelling relaxation data collected on a more concentrated sample of $^{4}$F1$^{5}$F1 (approximately 2 mM; data not shown) required a bead radius of 3.5 Å

TABLE 2
ROTATIONAL DIFFUSION CONSTANTS AND DERIVED CORRELATION TIMES CALCULATED FOR AN ENSEMBLE OF 32 $^4$F1$^5$F1 SIMULATED ANNEALING STRUCTURES

| Parameter[a] | Average | Standard deviation |
|---|---|---|
| $D_{xx}$ [b] | 2.59 | 0.12 |
| $D_{yy}$ | 2.63 | 0.11 |
| $D_{zz}$ | 4.95 | 0.10 |
| $D_\parallel/D_\perp$ [c] | 1.90 | 0.12 |
| $\tau_1$ [d] | 4.00 | 0.05 |
| $\tau_2$ | 5.56 | 0.15 |
| $\tau_3$ | 6.39 | 0.27 |
| $\tau_{c,eff}$ | 4.92 | 0.08 |

[a] $D_{xx}$, $D_{yy}$ and $D_{zz}$ are in units of $10^7$ s$^{-1}$; $\tau$ values are in units of ns.
[b] $D_{xx}$, $D_{yy}$ and $D_{zz}$ are the eigenvalues of the rotational diffusion tensor.
[c] $D_\parallel/D_\perp$ is approximated by $2D_{zz}/(D_{xx}+D_{yy})$.
[d] $\tau_{1,2,3}$ and $\tau_{c,eff}$ are the correlation times as defined by Barbato et al. (1992).

and a 1.6 Å half-shell of water, the same parameters used in the early studies (Venable and Pastor, 1988). In fact, diluting the $^4$F1$^5$F1 sample fourfold led to a 30% drop in the apparent correlation time, thereby reducing potential errors related to aggregation. The rotational diffusion tensor obtained for the ensemble of 32 $^4$F1$^5$F1 simulated annealing structures showed significant anisotropy, with an average tensor ratio of 1.0:1.9 (see Table 2). As expected, the anisotropy effect increases with field strength, so that at a $^{15}$N frequency of 76 MHz, relative variations in the $T_1/T_2$ ratio for $^4$F1$^5$F1 as large as 25% can be explained by anisotropy alone (see Fig. 4). However, inordinately high $T_1/T_2$ values at all frequencies, which were not fitted with the anisotropic model (see Fig. 2C), required the addition of a chemical exchange term in the relaxation analysis, as described in the next section.

## Determination of chemical exchange from measurements at three fields

So far, most $^{15}$N relaxation studies of proteins have relied on somewhat arbitrary criteria to locate sites undergoing chemical exchange; for relaxation measurements performed only at a single frequency, the introduction of the chemical exchange term, $R_{ex}$, into the Lipari–Szabo fitting of $T_2$ data may be misleading. Several approaches have been developed to quantify the effect of intramolecular chemical exchange by NMR, each of which can probe a different range of exchange rates. These methods include lineshape analysis (Ernst et al., 1986), $T_2$ measurements as a function of the refocussing delay in a CPMG spin-locking pulse sequence (Gutowsky et al., 1965; Carver and Richards, 1972; Davis et al., 1994) and $T_{1\rho}$ measurements as a function of the spin-lock rf field strength (Deverell et al., 1970). However, the quantitative application of these methods to a $^{15}$N-labelled protein sample is not straightforward. Significant line broadening is often observed for some resonances in 2D $^{15}$N-$^1$H correlated spectra of proteins; this can be attributed to the effect of intramolecular chemical exchange in the fast exchange limit. However, the lack of an appropriate model for the chemical exchange process will usually preclude further analysis. The application of the Carr–Purcell or $T_{1\rho}$ methods to a $^{15}$N-$^1$H scalar coupled spin system is further complicated either by the effect of scalar coupled free precession during the CPMG interpulse delay, if $2\tau$ becomes greater than about 1.6 ms, or in the general case by off-resonance effects if the rf field strength is reduced to a value comparable to the $^{15}$N offsets.

To identify intramolecular chemical exchange contributions in a protein sample, an exchange contribution is often included in the transverse relaxation rate of the $^{15}$N $T_2$ if the following condition applies (Tjandra et al., 1995):

$$\frac{T_{1,n}}{\langle T_1 \rangle} - \frac{T_{2,n}}{\langle T_2 \rangle} > 1.5\mathrm{SD} \qquad (1)$$

where $T_{i,n}$ is the $^{15}$N $T_1$ or $T_2$ value for residue n, and $\langle T_i \rangle$ is the average value over all residues. SD is the standard deviation of the quantity on the left-hand side of Eq. 1. Applied to the present case, this method identified four residues (residues 15, 25, 38 and 40) as subject to conformational exchange at all three frequencies. However, besides being somewhat arbitrary, this approach does not allow one to quantify $R_{ex}$, nor to include the effect of anisotropy.

We outline here an alternative approach to identify exchange contributions. It involves measurement of $^{15}$N $T_1$ and $T_2$ relaxation rates at three different magnetic field strengths. Similar considerations have been noted recently in the multiple magnetic field-dependent relaxation study of eglin c (Peng and Wagner, 1995) and in the relaxation data of Drk SH3 domain reported by Farrow et al. (1995). This approach is designed to exploit the anticipated quadratic field dependence of the exchange contribution to $^{15}$N transverse relaxation in the fast exchange limit. To illustrate this point, a simulation was performed, in the absence of a CPMG pulse sequence, to calculate the effect of chemical exchange on the observed transverse relaxation rate, $T_{2obs}$, over a range of values for the exchange rate k (Kaplan and Fraenkel, 1980). A two-site intramolecular rearrangement was assumed, with equal transverse relaxation rates of 8 s$^{-1}$ for each site and identical forward and backward rate constants. The simulations, shown in Fig. 5, were obtained for chemical shift differences between the two sites of 50.6, 60.8 and 76 Hz (dotted, dashed and solid curves, respectively). The slowest rate constant k used for each calculation was 1.5 times the chemical shift difference, to ensure that the fast exchange, single resonance, limit is valid. In each case, the

simulations indicate an observed additional rate, to the initially set $1/T_2$ rate of 8 $s^{-1}$, that depends on $\Delta\omega^2$ and decreases with increasing k. Below these curves are the simulated $1/T_2$ rates calculated with a CPMG pulse sequence using a value for $2\tau$ of 650 μs (Carver and Richards, 1972; Davis et al., 1994). As in the previous simulation, the $\Delta\omega^2$ dependence of the additional rate, due to chemical exchange, to the observed transverse relaxation rate is still valid for exchange rates, k, in the range $10^3$–$10^5$ $s^{-1}$. However, the introduction of the CPMG sequence adds a further complication to the determination of the rate constant k from the exchange contribution: the observed transverse relaxation rate could correspond to either of two values of k. Taking these limitations into account, we extracted the exchange contribution from our relaxation data at three frequencies in the following manner. Using the standard expressions for $^{15}N$ $1/T_1$ $(=R_1)$ and $1/T_2$ $(=R_2)$ relaxation rates (Abragam, 1961), the parameter $\{R_2 - R_1/2\}$ can be expressed as:

$$\left\{R_2 - \frac{R_1}{2}\right\} = \frac{c^2 + d^2}{3}J(0) + \frac{d^2}{2}J(\omega_H) + R_{ex} \quad (2)$$

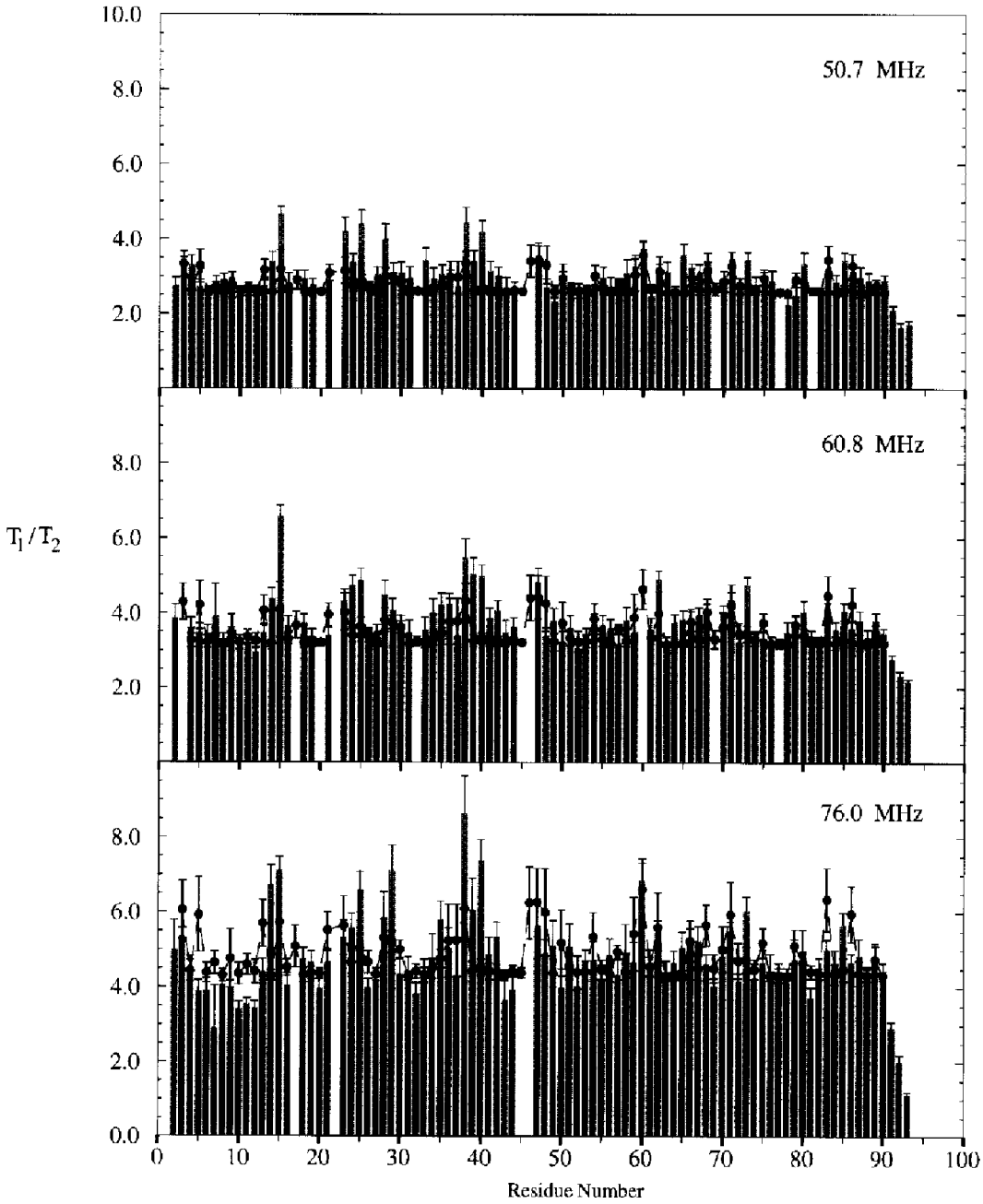


Fig. 4. Anisotropic modelling of $^4$F1$^5$F1 at three frequencies, using the beads model. Average back-calculated $T_1/T_2$ ratios are shown as filled circles, while experimental $T_1/T_2$ values appear as grey bars. Error bars on the back-calculated data represented by black bars and whiskers correspond to the $T_1/T_2$ standard deviation over 32 solution structures. The $^{15}N$ frequency is indicated in the top right-hand corner of each plot.

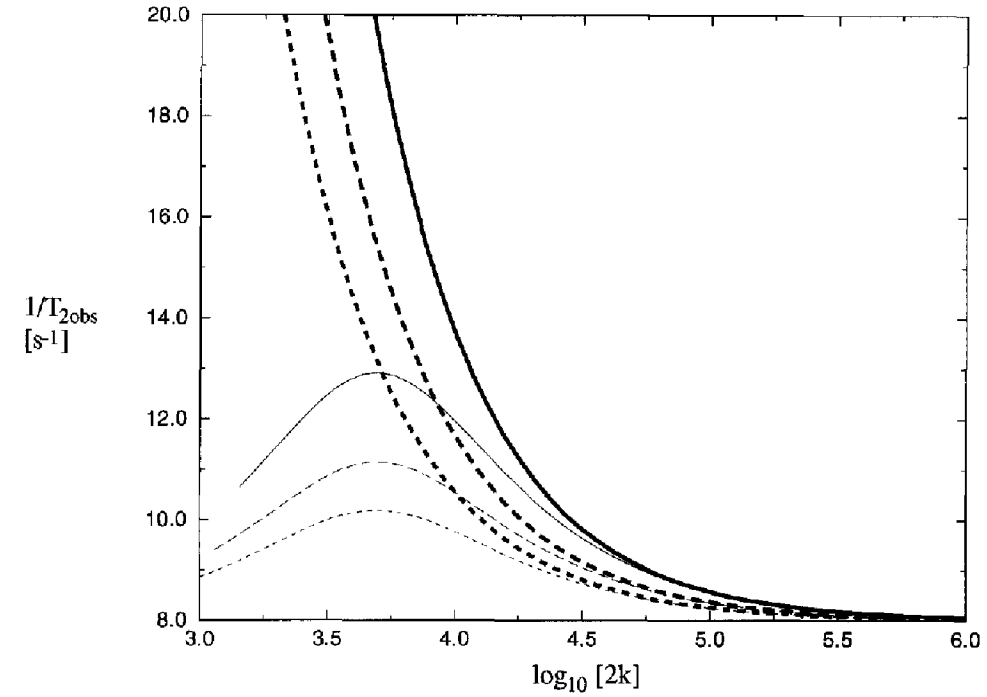


Fig. 5. Simulation of the chemical exchange effect on the observed transverse relaxation rate, $T_{2obs}$, as a function of the exchange rate, k (see text), at 50.8, 60.8 and 76.0 MHz (dotted, dashed and solid curves, respectively). Thick curves correspond to simulations in the absence of a CPMG pulse sequence.

where $d = -(\mu_0/4\pi)(6\pi/5)^{1/2}\,(\gamma_N\,\gamma_H\hbar/r_{NH}^3)$, $c = (8\pi/15)^{1/2}\,\gamma_N\,B_0(\sigma_\parallel - \sigma_\perp)$; $\tau_i$ is the gyromagnetic ratio of spin i, $\hbar$ is Planck's constant divided by $2\pi$, $r_{NH}$ (=0.101 nm) is the NH bond length, $\mu_0$ ($=4\pi 10^{-7}$ kg m $s^{-2}$ $Å^{-2}$) is the permea-

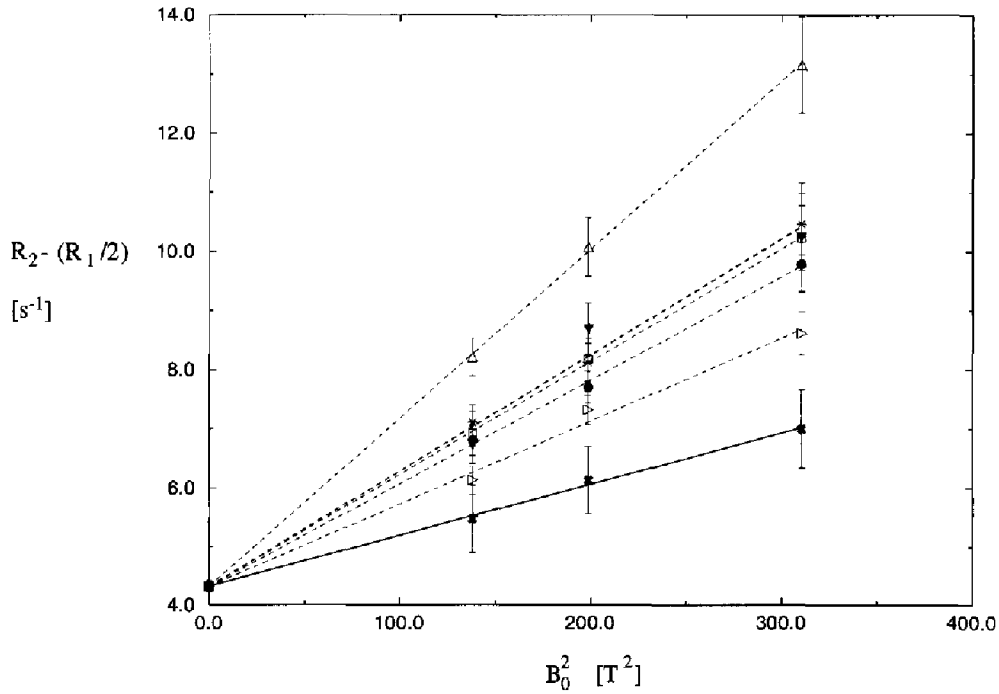


Fig. 6. Plot of $\{R_2 - R_1/2\}$ versus $B_0^2$ for the experimental determination of the chemical exchange rate $R_{ex}$. For clarity purposes, all fitted data sets have been scaled to the intercept $I_0$ of the average fit for non-exchanging residues, so that only differences in the slope are shown. Experimental values per residue are represented by the following symbols: $Val^{14}$, filled circle; $Val^{29}$, open square; $Ser^{38}$, open triangle up; $Gly^{39}$, filled triangle down; $Arg^{40}$, star; $Arg^{48}$, open triangle. Average values for non-exchanging residues are shown as an X. Bars and whiskers represent the experimental error and dotted lines the slope from the linear regression for each data set. The linear regression for non-exchanging residues is shown as a thick line.

TABLE 3
CHEMICAL EXCHANGE RATES FOR $^4$F1$^5$F1

| Residue | $\tau_m S^2$ (ns) | $R_{ex}$ ($s^{-1}$) for various $B_0$ (T)[a] | | |
|---|---|---|---|---|
| | | 11.7466 (50.7) | 14.0954 (60.8) | 17.6203 (76.0) |
| Val[14] | 3.6 | 1.6 | 2.3 | 3.6 |
| Val[29] | 3.3 | 1.9 | 2.7 | 4.2 |
| Ser[38] | 3.1 | 3.2 | 4.7 | 7.3 |
| Gly[39] | 3.8 | 1.8 | 2.6 | 4.1 |
| Arg[40] | 4.5 | 1.7 | 2.4 | 3.8 |
| Arg[48] | 2.9 | 1.3 | 1.8 | 2.9 |
| Average non-exchanging | 3.9 | 0.6 | 0.9 | 1.4 |

The chemical exchange rates were calculated from the coefficients of the linear function $\{R_2 - R_1/2\}$ versus $B_0^2$. The second column gives the product of the correlation time, $\tau_m$, and the order parameter, $S^2$, obtained from the intercept.

[a] The $^{15}$N Larmor frequency, in MHz, is given in parentheses.

bility of free space, $B_0$ is the magnetic field strength, $\sigma_\parallel$ and $\sigma_\perp$ are the parallel and perpendicular components of the axially symmetric $^{15}$N chemical shift tensor ($\sigma_\parallel - \sigma_\perp = -160$ ppm), and $J(\omega_i)$ is the spectral density function at frequency $\omega_i$. The second term of Eq. 2 is frequency dependent. However, with the assumption of an exponentially decaying autocorrelation function (Abragam, 1961) and using realistic values for $S_2$, $\tau_m$ and with $R_{ex} \geq 1\ s^{-1}$, the second term is small in comparison with the others and can reasonably be neglected. Equation 2 can now be rearranged to exhibit a quadratic dependence by introducing $R_{ex} = A B_0^2$, where $B_0$ is the field strength and A is a constant, and setting $c_1 = c/B_0 = (8\pi/15)^{1/2}\gamma_N(\sigma_\parallel - \sigma_\perp)$:

$$\left\{R_2 - \frac{R_1}{2}\right\} \approx \left(\frac{c_1^2}{3}J(0) + A\right)B_0^2 + \frac{d^2}{3}J(0) \qquad (3)$$

Using a plot of $\{R_2 - R_1/2\}$ versus $B_0^2$, the spectral density function J(0) can be deduced from the intercept, i.e., $I_0 = d^2\,J(0)/3$. The exchange constant A is then calculated from the slope $m = [J(0)c_1^2/3] + A$, so that Eq. 4 is obtained:

$$A = m - \frac{c_1^2 I_0}{d^2} \qquad (4)$$

Thus, any spin for which the data has a slope $m > (c_1^2 I_0/d^2)$ will have an exchange contribution $A B_0^2$ to its transverse relaxation rate. With this method, six residues were identified as subject to conformational exchange and the $R_{ex}$ terms were calculated (see Fig. 6 and Table 3). However, taking into consideration experimental and fitting errors arising from extracting a slope and intercept from a linear regression to only three data points, the condition $A = 0$ for all non-exchanging residues could not be strictly applied. We observed that only data for 45 residues (56%) fitted a straight line with positive slope within experimental errors. Practically, the analysis was conducted for 31 residues (37%) for which the slopes between the 50.6 and

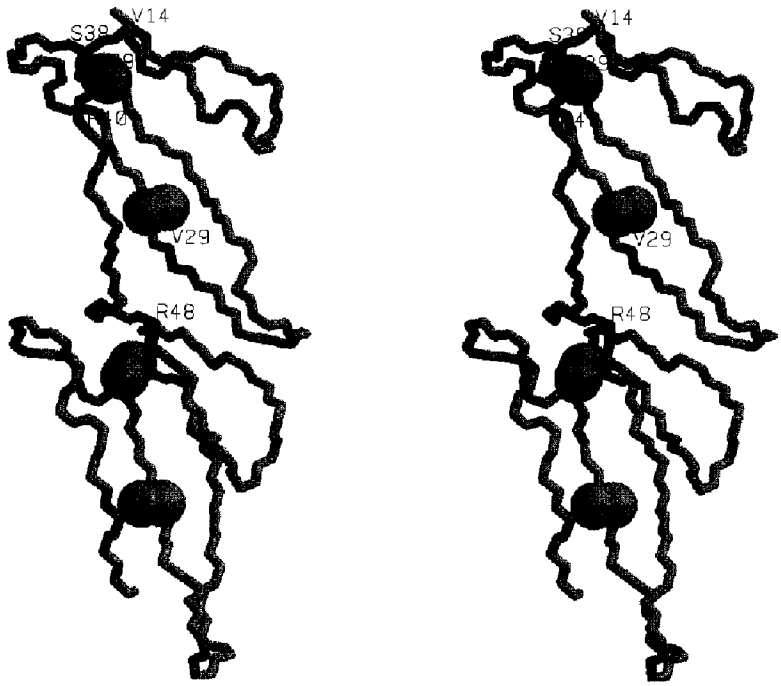


Fig. 7. Stereoview of the backbone structure of an average $^4$F1$^5$F1 solution structure. Residues undergoing chemical exchange, where the exchange contribution shows a quadratic field dependence, are coloured in black and their sequence numbers are indicated. Sulphur atoms of cysteine residues involved in disulphide bridges (between residues 4–33, 31–44, 49–78, 76–88) are displayed as spheres. This picture was produced using the RasMol2.6b2 molecular viewer written by Roger Sayle.

60.8 MHz data, and the 50.6 and 76.0 MHz data, differed by less than 40%. A threshold of 1.3*<m> was then used to determine residues subject to conformational exchange, where <m> is the average slope.

In the present approach, no model-based assumption (see earlier) is made for the spectral density function. However, if the Lipari–Szabo model, with variable $\tau_m$ to account for anisotropy, is used so that $J(0) = S^2 \tau_m / 2\pi$, then the product $\tau_m S^2$ can be extracted from the intercept $I_0$:

$$\tau_m \, S^2 = \frac{5}{10^{-14}} \left( \frac{r_{NH}^3}{\gamma_N \gamma_H h} \right)^2 I_0 \qquad (5)$$

The average value for the intercept for those residues not involved in chemical exchange was found to be $4.24 \pm 0.09$ $s^{-1}$. Assuming a value of 0.8 for $S^2$, this would give an apparent overall correlation time of $4.81 \pm 0.10$ ns, which is in very good agreement with the values obtained from the theoretical models. Figure 7 shows the location on an average $^4$F1$^5$F1 structure of residues subject to conformational exchange, where the exchange contribution displays a quadratic field dependence. These residues seem to be located mainly in spatial proximity to the disulphide bridge between cysteines 4 and 33, which could be an indication of cystine bond isomerism, an effect that has already been observed in some proteins with disulphide bonds (Szyperski et al., 1993). It is interesting to note that this effect is only seen in the first of the two fibronectin type I modules, although both modules share the same tertiary fold and the same disulphide bond pattern.

## Conclusions

This relaxation analysis has clearly shown that the module pair $^4$F1$^5$F1 from fibronectin can be modelled fairly well by a cylinder of axial ratio 1.9. This model is particularly impressive, because it applies to data collected at three frequencies. A field-dependent analysis is presented for detecting the exchange contribution to relaxation. With this method, six residues were identified as subject to conformational exchange, mainly located in the vicinity of one of the four disulphide bonds of the module pair.

## Acknowledgements

We thank Michael J. Williams for producing the $^4$F1$^5$F1 sample labelled with $^{15}$N. We also thank Arthur Palmer III for providing the Modelfree package and Victor Bloomfield for making the HYDRO program freely available. Christina Redfield, Jörn Werner and Jonathan Jones are gratefully acknowledged for their help in performing the Lipari–Szabo analysis. The OCMS is supported by BBSRC, MRC and EPSRC. I.D.C. also acknowledges support from the Wellcome Trust.

## References

Abragam, A. (Ed.) (1961) *The Principles of Nuclear Magnetic Resonance*, Clarendon Press, Oxford, U.K.

Barbato, G., Ikura, M., Kay, L.E., Pastor, R.W. and Bax, A. (1992) *Biochemistry*, **31**, 5269–5278.

Bork, P. and Bairoch, A. (1995) *Trends Biochem. Sci.*, 02 (Supplement).

Bork, P., Downing, A.K., Kieffer, B. and Campbell, I.D. (1996) *Q. Rev. Biophys. Biochem.*, **29**, 119–167.

Boyd, J., Hommel, U. and Campbell, I.D. (1990) *Chem. Phys. Lett.*, **175**, 477–481.

Brüschweiler, R., Liao, X. and Wright, P.E. (1995) *Science*, **268**, 886–889.

Campbell, I.D. and Downing, A.K. (1994) *Trends Biotechnol.*, **12**, 168–172.

Carver, J.P. and Richards, R.T. (1972) *J. Magn. Reson.*, **6**, 89–105.

Clore, G.M., Szabo, A., Bax, A., Kay, L.E., Driscoll, P.C. and Gronenborn, A.M. (1990) *J. Am. Chem. Soc.*, **112**, 4989–4991.

Davis, D.G., Perlman, M.E. and London, R.T. (1994) *J. Magn. Reson.*, **104**, 266–275.

Deverell, C., Morgan, R.E. and Strange, J.H. (1970) *Mol. Phys.*, **18**, 553–559.

Ernst, R.R., Bodenhausen, G. and Wokaun, A. (Eds.) (1986) *Principles of Nuclear Magnetic Resonance in One and Two Dimensions*, Oxford University Press, Oxford, U.K.

Farrow, N.A., Muhandiram, R., Singer, A.U., Pascal, S.M., Kay, C.M., Gish, G., Schoelson, S.E., Pawson, T., Forman-Kay, J.D. and Kay, L.E. (1994) *Biochemistry*, **33**, 5984–6003.

Farrow, N.A., Zhang, O., Szabo, A., Torchia, D.A. and Kay, L.E. (1995) *J. Biomol. NMR*, **6**, 153–162.

García de la Torre, J. and Bloomfield, V.A. (1981) *Q. Rev. Biophys.*, **14**, 81–139.

García de la Torre, J., Navarro, S., Lopez Martinez, M.C., Diaz, F.G. and Lopez Cascales, J.J. (1994) *Biophys. J.*, **67**, 530–531.

Gutowsky, H.S., Vold, R.L. and Wells, E.J. (1965) *J. Chem. Phys.*, **43**, 4107–4125.

Kaplan, J.I. and Fraenkel, G. (Eds.) (1980) *NMR of Chemically Exchanging Systems*, Academic Press, New York, NY, U.S.A.

Kay, L.E., Torchia, D.A. and Bax, A. (1989) *Biochemistry*, **28**, 8972–8979.

Lipari, G. and Szabo, A. (1982) *J. Am. Chem. Soc.*, **104**, 4546–4570.

Matsuka, Y.V., Medved, L.V., Brew, S.A. and Inghams, K.C. (1994) *J. Biol. Chem.*, **269**, 9539–9546.

Oas, T.G., Hartzell, C.J., Dahlquist, F.W. and Drobny, G.P. (1987) *J. Am. Chem. Soc.*, **109**, 5962–5966.

Pawson, T. (1995) *Nature*, **373**, 573–580.

Peng, J. and Wagner, G. (1995) *Biochemistry*, **34**, 16733–16752.

Potts, J.R. and Campbell, I.D. (1994) *Curr. Opin. Cell Biol.*, **6**, 648–655.

Rostagno, A., Williams, M.J., Baron, M., Campbell, I.D. and Gold, L.I. (1994) *J. Biol. Chem.*, **269**, 31938–31945.

Schurr, J.M., Babcock, H.P. and Fujimoto, B.S. (1994) *J. Magn. Reson.*, **B105**, 211–224.

Szyperski, T., Luginbühl, P., Otting, G., Güntert, P. and Wüthrich, K. (1993) *J. Biomol. NMR*, **3**, 151–164.

Tjandra, N., Feller, S.E., Pastor, R.W. and Bax, A. (1995) *J. Am. Chem. Soc.*, **117**, 12562–12566.

Venable, R.M. and Pastor, R.W. (1988) *Biopolymers*, **27**, 1001–1014.

Williams, M.J., Phan, I., Harvey, T.S., Rostagno, A., Gold, L.I. and Campbell, I.D. (1994) *J. Mol. Biol.*, **235**, 1302–1311.

Woessner, D.E. (1962a) *J. Chem. Phys.*, **36**, 1–4.

Woessner, D.E. (1962b) *J. Chem. Phys.*, **37**, 647–654.

Zheng, Z., Czaplicki, J. and Jardetzky, O. (1995) *Biochemistry*, **34**, 5212–5223.